Subtle pH variation around pH 4.0 affects aggregation kinetics and aggregate characteristics of recombinant human insulin

Thorlaksen, C.; Stanciu, A.M.; Busch Neergaard, M.; Jiskoot, W.; Groenning, M.; Foderà, V.

European Journal of Pharmaceutics and Biopharmaceutics 179 (2022) 166–172

Contents lists available at ScienceDirect

European Journal of Pharmaceutics and Biopharmaceutics

journal homepage: www.elsevier.com/locate/ejpb

Subtle pH variation around pH 4.0 affects aggregation kinetics and aggregate characteristics of recombinant human insulin

Camilla Thorlaksen [a,b,*], Adriana-Maria Stanciu [a,b], Martin Busch Neergaard [a], Wim Jiskoot [c], Minna Groenning [a,1,*], Vito Foderà [b,1,*]

[a] Biophysical analysis, Novo Nordisk A/S, Novo Nordisk Park 1, 2760 Måløv, Denmark
[b] Department of pharmacy, University of Copenhagen, Universitetsparken 2, 2100 Copenhagen, Denmark
[c] Division of BioTherapeutics, Leiden University, Einsteinweg 55, 2300 RA Leiden, Netherlands

ARTICLE INFO

Keywords:
Particulates
Human insulin
Aggregates
Particles
pH

ABSTRACT

Insulin is a biotherapeutic protein, which, depending on environmental conditions such as pH, has been shown to form a large variety of aggregates with different structures and morphologies. This work focuses on the formation and characteristics of insulin particulates, dense spherical aggregates having diameters spanning from nanometre to low-micron size. An in-depth investigation of the system is obtained by applying a broad range of techniques for particle sizing and characterisation. An interesting observation was achieved regarding the formation kinetics and aggregate characteristics of the particulates; a subtle change in the pH from pH 4.1 to pH 4.3 markedly affected the kinetics of the particulate formation and led to different particulate sizes, either nanosized or micronsized particles. Also, a clear difference between the secondary structure of the protein particulates formed at the two pH values was observed, where the nanosized particulates had an increased content of aggregated β-structure compared to the micronsized particles. The remaining characteristics of the particles were identical for the two particulate populations. These observations highlight the importance of carefully studying the formulation design space and of knowing the impact of parameters such as pH on the aggregation to secure a drug product in control. Furthermore, the identification of particles only varying in few parameters, such as size, are considered highly valuable for studying the effect of particle features on the immunogenicity potential.

1. Introduction

Insulin is a biotherapeutic protein, which has been shown to form aggregates including amyloid-like fibrils, spherulites and particulates [1–5]. While the amyloid-like fibrils have a linear symmetry with a diameter of a few nanometres and a micrometric length [6,7], spherulites and particulates are spherical aggregates [1]. Spherulites consist of amyloid-like elongated structures extending from a core and have a diameter ranging from a few microns to millimetres [4,8,9], whereas particulates consist of compact spherical particles with a diameter of 100 nm to 2 μm [10,11]. These aggregate types appear to be common in a variety of proteins [12–16], and the formation of the specific protein superstructure depends on environmental conditions such as solvent pH and elevated temperatures [3,9,17]. Spherulites and amyloid-like fibrils form at acidic pH [18,19], while particulates often form near the protein's isoelectric point (pI) [11,16].

Health authorities are increasingly concerned about protein particles in therapeutic injectables [20–22], since they have been shown to be associated with an increased risk of immunogenic events [23–26]. Particle characteristics such as size, shape, physicochemical properties, higher order structure, and dissociation have been found to likely impact the immunogenicity [27–32]. Specifically, the amount of investigative work on the impact of size illustrates the importance of this relation [23,33–37]. However, there is currently no consensus of what particle size range results in the highest immunogenicity risk [30]. Particle size and aggregation propensity of spherulites have been shown to be affected as a consequence of even minute changes in pH (0.1 units) [3]. However, an extensive investigation of whether small changes in pH around pH 4.0 can impact formation kinetics and characteristics of particulates formed from insulin has to our knowledge not been performed.

In the present study, an in-depth examination and characterisation of

* Corresponding authors.
E-mail addresses: cdbt@novonordisk.com (C. Thorlaksen), mgqj@novonordisk.com (M. Groenning), vito.fodera@sund.ku.dk (V. Foderà).
[1] These authors share last authorship of the manuscript.

https://doi.org/10.1016/j.ejpb.2022.09.001
Received 25 May 2022; Received in revised form 30 August 2022; Accepted 2 September 2022
Available online 8 September 2022

the insulin particulate system is obtained by combining the information from a broad range of biophysical techniques to study size, shape, and structure. Specifically, we show, by combining Micro-Flow Imaging (MFI) and Resonant Mass Measurements (RMM), that subtle changes (in the range of a few decimals) in pH in the vicinity of the pI of insulin, results in a pronounced variability in the size of the particulates formed. Moreover, Scanning Electron Microscopy (SEM) and Fourier Transform Infrared spectroscopy (FTIR) was used to report morphologically similar particles with a pH dependent change in secondary structure.

Our results emphasize the significance of a highly accurate pH control for drug product formulations to avoid the activation of different aggregation pathways and thus formation of product related impurities with different size and secondary structure. Moreover, our findings highlight the importance of using a plethora of techniques to thoroughly characterise the formed aggregates and thereby provide a more complete picture of the aggregate landscape during stress tests.

2. Materials and methods

2.1. Solvent and sample preparation

The solvent used for producing particulates was prepared by dissolving sodium acetate trihydrate powder (≥99.0 %, Merck KGaA, Darmstadt, Germany) in reverse-osmosis water (Milli-Q) to a final concentration of 20 mM. The solvent was filtered through a 0.1 μm PES filter mounted directly onto a 50 mL centrifuge tube (#514–0366, VWR, Radnor, PA, USA) before use in sample preparations. Zinc-complexed recombinant human insulin was kindly provided by Novo Nordisk A/S (Måløv, Denmark) as a lyophilized powder. For sample preparation, 20 mM sodium acetate solution was added to the human insulin for a final protein concentration of 5 mg/mL. At this stage, the sample solution appeared turbid (white), due to the limited solubility of insulin near its pI. To dissolve the insulin, 1 M HCl (99.0 %, Merck KGaA, Darmstadt, Germany) was gently added to the sample solution until pH 2.2 was reached. Once dissolved, the solution pH was increased using 1 M NaOH (99.0 %, Merck KGaA, Darmstadt, Germany) to reach its target pH in the range from 4.0 to 4.3, depending on the assay. Swirling motions were applied in-between pH titrations to ensure proper mixing and stable pH measurements. The sample solutions were filtered through a low protein binding 0.1 μm inorganic membrane filter (#6809–2012, Whatman, Little Chalfont, UK) by using a silicone- and latex-free syringe (#4050-X00V0, Henke Sass Wolf, Tuttlingen, Germany) into a Nunc 15 mL conical centrifuge tube (#339651, Thermo Fisher Scientific, Waltham, MA, USA), while ensuring a continuous flow down the side of the tube to avoid pre-aggregation [38]. The filter and syringe had been pre-washed x3 with water. Aliquots of 1 mL of sample solution was added to 1.5 mL Eppendorf tubes (#0030 120.086, Eppendorf AG, Hamburg, Germany) and subsequently placed into a thermomixer (thermomixer comfort, Eppendorf AG, Hamburg, Germany) at 80 °C for 2.5 h for stress application.

2.2. Aggregation kinetics

Aggregation kinetics were followed by measuring the amount of free non-aggregated insulin as a function of time, while applying stress to the sample. First, samples at pH 4.0 and 4.3 were prepared and their initial protein concentration was determined ($\lambda_{276\ nm}$) by using a NanoDrop 2000c Spectrophotometer (Thermo Scientific, Waltham, MA, USA). Next, the sample solutions were divided into 12 Eppendorf tubes each (1 mL/tube) and placed into a thermo heater (digital heating block, VWR, Radnor, PA, USA) at 80 °C. At each specified time point, a sample was taken from the heating block, centrifuged (5417R, Eppendorf, Hamburg, Germany) at 13,000 rpm, 4 °C for 20 min and the protein concentration of the supernatant was determined. Data were collected by using the NanoDrop 2000/2000c software. Percentage conversion into particles as a function of time was calculated as $(C_{initial} - C_{supernatant} / C_{initial})*100$.

2.3. Flow Imaging Microscopy

Unstressed and stressed samples were analysed with a Micro-Flow Imaging microscope (model 5200, ProteinSimple, ON, Canada) by using a method setup having no prior sample purging and a manual stop function. This allowed for analysing small sample volumes (approx. 300 μL), to enable the use of multiple techniques for characterisation of the same sample. Before analysis, the flow cell (#4002–002-001, 100 μm, silane coating, ProteinSimple, Toronto, ON, Canada) was cleaned with 2% Hellmanex (v/v) and water until the instrument was clean enough to obtain a baseline particle concentration of < 150 #/mL. The illumination was automatically optimised by the instrument to remove any particle impurity adhered to the flow cell and adjust detector settings in the field-of-view. Unstressed samples were measured without dilution and the illumination was hereby optimised on 20 mM sodium acetate solution adjusted to pH of the analysed sample. This was done to ensure that the sample would not precipitate inside the flow cell due to small pH differences. Whereas stressed samples were diluted in water (x100 dilution for pH 4.1 samples, x50 dilution for pH 4.3 samples) before measurements due to their stability and the illumination was hereby optimised on water. Between measurements of different samples, the instrument was cleaned with 2% Hellmanex (v/v) and water. For data evaluation an in-house developed software was used [39]. The first 250 frames were discarded to avoid artificial dilution. The estimated Equivalent Circular Diameter (ECD, μm) for each particle was used to determine size distribution differences, homogeneity, and preparation reproducibility among the samples.

2.4. Resonant Mass measurements

Stressed samples prepared at pH 4.1 and 4.3 were analysed with an Archimedes system (RMM2001, Affinity Biosensors, Santa Barbara, CA, USA) equipped with a microH sensor (range 200 nm-5 μm, Malvern Instruments, Malvern, UK) for particle detection. Prior to sample analysis, the sensor was aligned and calibrated by using 1.0 μm polymer microspheres (NIST traceable 0.994 μm ± 0.021 μm, #4009A, Duke Scientific Corporation, Freemont, CA, USA). Samples were diluted in water (x500 dilution for pH 4.1 samples, x5 dilution for pH 4.3 samples) before being loaded into the sensor for 25–30 s. During measurements, the limit-of-detection was set to be calculated automatically by the software and it was ensured that the particle coincidence was kept below 5% for all samples. The density used for sensor calibration experiments was 1.05 g/cm^3. For sample analysis, a density of 1.34 g/cm^3 was used for protein particles (negative buoyant material) [40–42] and 0.971 g/cm^3 for potential silicone oil droplets (positive buoyant material). Since samples were diluted in water, the density and viscosity of water were used for all measurements. For each sample, 1000 particles were recorded using the ParticleLab software version 1.9.81. Only particles with negative buoyancy (protein particles) were used for further data treatment. The system was cleaned with 2–3 “sneeze” operations while loading 2% PCC-54 (detergent concentrate, #72288, Thermo Scientific, Waltham, MA, USA), followed by loading of water in between samples.

2.5. Optical, polarization and fluorescence Microscopy

Samples containing particulates prepared at pH 4.3 were stained with 30 μM Thioflavin T dye (≥65 %, T3516, Sigma Aldrich, Saint Louis, MO, USA). Subsequently, 80 μL sample was deposited into a microscope chamber slide made by adhering a 6-channelled sticky slide VI 0.4 (#80608, Ibidi GmbH, Martinsried, Germany) together with a cover glass slide (1.5 mm thickness, Menzel-Gläser, VWR, Radnor, PA, USA). Imaging was performed with a Leica DMi8 microscope (Triolab A/S, Brøndby, Denmark), allowing for optical, polarization and fluorescence detection in the same field-of-view at a 1920x1440 pixel resolution using a 63x oil immersion objective (63x/1.30 oil objective, high NA, HC PL FLUOTAR, #11506384, Triolab A/S, Brøndby, Denmark). For optical

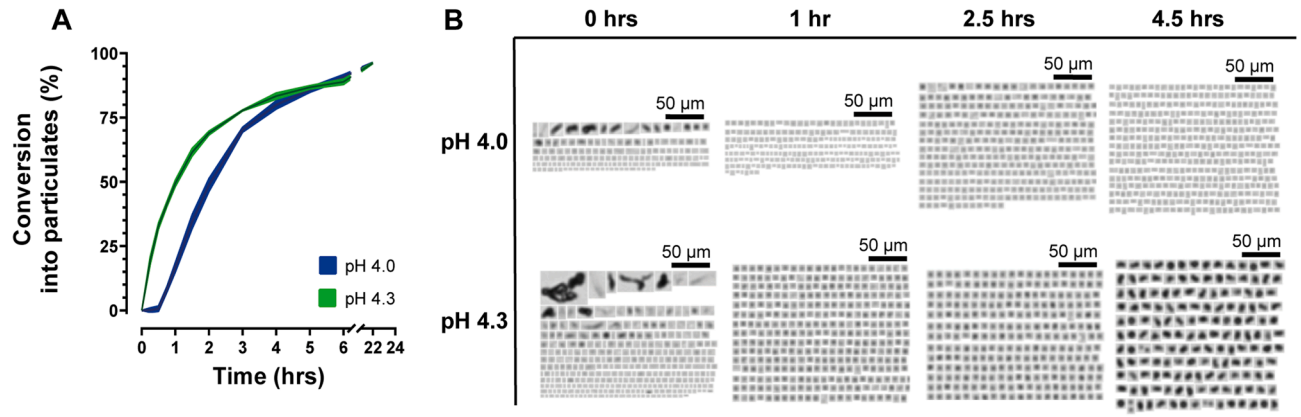

Fig. 1. Kinetics and morphology during particulate formation. A) Kinetic measurements for two pH values, pH 4.0 (blue line) and 4.3 (green line). Concentration of free human insulin in the supernatant as a function of stress time is utilized as a reverse measure of particulate formation. The percentage conversion is calculated based on the initial protein concentration at t=0. The shaded errors are standard deviation of three independent measurements. B) Representative MFI images showing morphology as a function of stress time. Samples prepared at either pH 4.0 or 4.3 were taken out of the incubator at different time points during the particulate formation and analyzed using MFI. This was to investigate the time point at which the formed particles were most individualized. The 17 hour and 24 hour timepoints can be viewed in Fig. S4.

and polarization applications, a LED3 lumencor light source "white light" (#11504254, Triolab A/S, Brøndby, Denmark) was used. Whereas fluorescence was obtained with a light fibre connection by filtering desired wavelengths for ThT fluorescence detection using a FITC bandpass (ex. 480/40, em. 527/30, #11525308, Triolab A/S, Brøndby, Denmark). Leica software platform LAS X was used for image acquisition and ImageJ for image processing.

2.6. Fourier-Transform InfraRed spectroscopy

Unstressed and stressed samples prepared at pH 4.1 and 4.3 were characterized for secondary structure features using a Tensor II Confocheck FTIR spectrophotometer with BioATR II module (Bruker Corporation, Billerica, MA, USA). Data acquisition was obtained with OPUS software version 7.5.18. Stressed samples were divided into supernatant and pellet by centrifugation (5417R, Eppendorf, Hamburg, Germany) at 14,000 rpm, 4 °C for 30 min. Before measurements, the ATR crystal was cleaned with deionized water and 70% ethanol (v/v). A background spectrum of 20 mM sodium acetate solution, with pH adjusted to the respective sample pH, was recorded prior to sample measurements, and automatically subtracted from sample measurements by the software. Absorbance spectra for the samples are an average of 512 scans recorded in range 900 cm^{-1} –4000 cm^{-1} with a 4 cm^{-1} resolution. The amide I band (1600 cm^{-1} – 1710 cm^{-1}) was used to evaluate structural differences between samples.

2.7. Scanning Electron Microscopy

Scanning Electron Microscopy measurements were carried out in high vacuum mode and the samples thus needed to be dried before analysis. To obtain enough material for imaging, samples prepared at pH 4.1 and 4.3 were stressed for 24 h (3 tubes pr. sample type) and subsequently centrifuged (5417R, Eppendorf, Hamburg, Germany) at 14,000 rpm, 4 °C for 30 min. Pellets from each sample type, containing the particulates, were pooled and dried on a glass slide for 48 h. The dried material was gently scratched off the glass slide onto a specimen stage with carbon tape (Agar Scientific Ltd, Essex, UK) and sputter coated with 0.2 nm gold using a Leica Coater ACE 200 (Leica Microsystems, Wetzlar, Germany). Imaging was performed using a FEI Quanta 3D FEG Scanning Electron Microscope (Thermo Fisher Scientific, Hillsboro, OR, USA) with an Everhart-Thornley Detector (ETD) and high-resolution dual beam. The acceleration voltage was 2.00 kV for all acquisitions.

3. Results and discussion

3.1. Particulate preparation details

The present study focuses on the formation and characteristics of insulin particulates formed in the vicinity of the pI of the protein and at elevated temperatures. The pI for human insulin is ~ 5.4 [43], however based on sample turbidity, we found that the insulin could not be dissolved above pH 4.4 in a 20 mM sodium acetate solution containing 5 mg/ml protein (Fig. S1). Thus, we investigated the narrow pH range from pH 4.0 to 4.3. The preparation is performed by dissolving human insulin at low pH (pH 2.2) before setting the final pH value (see Fig. S2 for a graphical illustration of the sample preparation protocol). Native insulin solutions at different pHs were analysed by dynamic light scattering with the aim of obtaining information on the insulin oligomeric state (see Fig. S3). For ideal measurement conditions, monomeric, dimeric and hexameric insulin will have a hydrodynamic radius (R_h) of 1.27 nm, 1.81 nm and 2.6 nm, respectively [44]. The data show a linear increase in the apparent (R_h) from 2.9 nm at pH 4.0 to 3.4 nm at pH 4.3. This may be indicative of the propensity of insulin to self-assembly at pHs closer to the pI and due to the suppression of the repulsive electrostatic interaction [13,45,46]. However, an effect of non-ideal measuring conditions on the DLS results cannot be ruled out. This would result in an artificially high apparent R_h due to attractive intermolecular interactions. A detailed description of the particulate preparation procedure at 5 mg/ml human insulin in 20 mM sodium acetate at pH 4.3 is also provided in a previous publication from our research group [38].

3.2. The kinetics of particulate formation depends on pH

Kinetics of the particulate formation were examined at each edge of the chosen pH interval, namely pH 4.0 and pH 4.3. Aggregation kinetics during heat stress were monitored by measuring the amount of free non-aggregated human insulin in the sample supernatant as a function of time. The method is a reverse measure of the percent conversion of protein into particulate formation. We observed that the kinetics at pH 4.0 had a lag-phase of 30 min, while no lag-phase could be detected for the kinetics at pH 4.3 (Fig. 1A). Moreover, the aggregation rate is slower at pH 4.0. This suggests two different aggregation pathways depending on subtle changes in the pH. To our knowledge such pronounced effect on the aggregation by subtle changes in pH has not previously been shown for preparations around pH 4.0. However, it has previously been

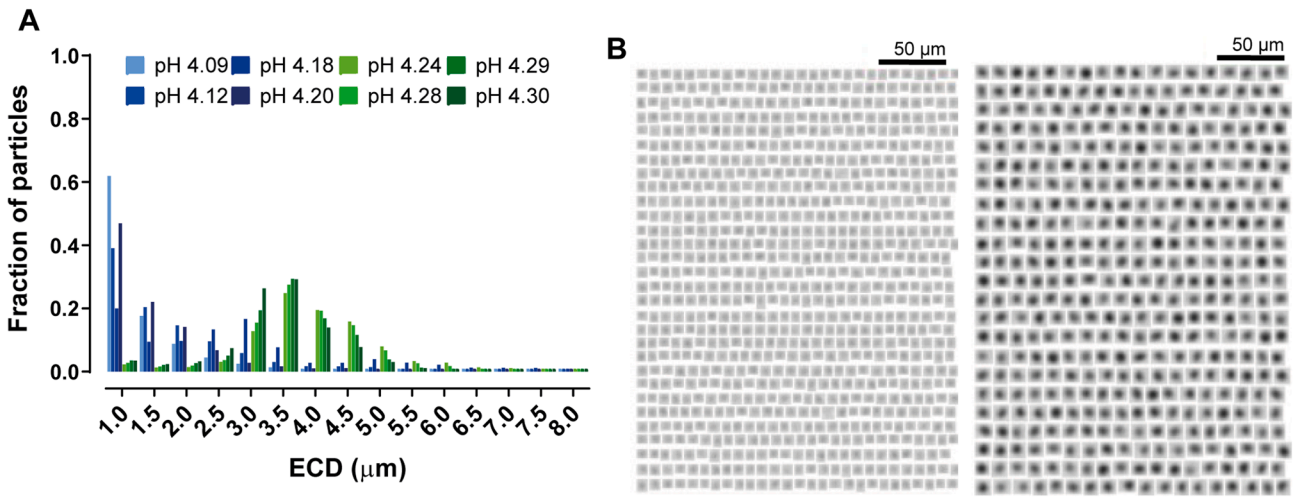

Fig. 2. Subtle changes in pH affect size of formed particulates. A) Fraction of particles as a function of size (measured as equivalent circular diameter (ECD)) for particulates formed under small increments of pH values ranging from pH 4.1 to pH 4.3 analyzed using MFI. B) Representative MFI images showing the morphology of particulates formed at pH 4.1 (left) and 4.3 (right), respectively.

reported for bovine insulin at extremely low pH values, where other types of aggregates were formed [3]. This emphasizes the important role of pH on the physical degradation pathway. We hypothesize that the different kinetics might be an effect of small changes in the protein net charge. To confirm our hypothesis of particulate formation in the conditions used and possible particle–particle clustering at various time points during the kinetics, we tracked particle formation using MFI during the heat stress test at 0 h, 1 h, 2.5 h, 4.5 h, 17 h, and 24 h (Fig. 1B and Fig. S4). Data showed that at time zero only a few particles were detected. These particles were comparable to the particles observed in a solution of 20 mM sodium acetate with no protein present (Fig. S5). These particles can thus not be ascribed to particulate formation, but more likely to minor dust/contaminants from preparation materials. A low number of spherical micron-sized particles were detected at pH 4.0 within the first 2.5 h. Smaller particles (<5μm) started to appear after 4.5 h, where 80% of the insulin was converted into particulates (Fig. 1B). Additional stress to the sample led to formation of larger particle–particle clusters (Fig. S4). A comparable pattern is seen for samples prepared at pH 4.3. However, and surprisingly, the faster aggregation rate at pH 4.3 allowed for detection of micron-sized particles already after 1 h. At this time, the particles appeared denser and larger than the particles seen at pH 4.0 (Fig. 1B). Stressing the sample for longer than 4.5 h led to initiation of particle–particle clustering (Fig. S4). For further in-depth characterisation of the particulates, conditions where individual particulates are present (no clustering) was considered ideal.

Therefore, based on the MFI kinetic results, we determined the most optimal stress test time to be 2.5 h for further studies, even though free non-aggregated insulin is present in the solution (40% and 26% free insulin at pH 4.0 and pH 4.3, respectively).

3.3. Particulate size depends on pH

We performed a quantitative analysis of the size distribution of the particulates formed in the pH range 4.1 to 4.3 using formulations in which the pH changes in the order of approx. 0.05 pH units. Surprisingly, the particle size shows a clear shift of the size distribution after 2.5 h stress time, when passing from pH 4.20 to pH 4.24 (Fig. 2A). For pH ≤ 4.20, we identify a main peak centred below 1 μm with a decay contribution for higher sizes (blue distributions in Fig. 2A). In fact, 71% of the total number of detected particles at pH 4.1 resides in the size range below 2 μm (Fig. S6). For pH > 4.20 the size distribution changes to a symmetric distribution centred around 3.5 μm (green distributions in Fig. 2A) with limited presence of particles < 2 μm. In fact, at pH 4.3

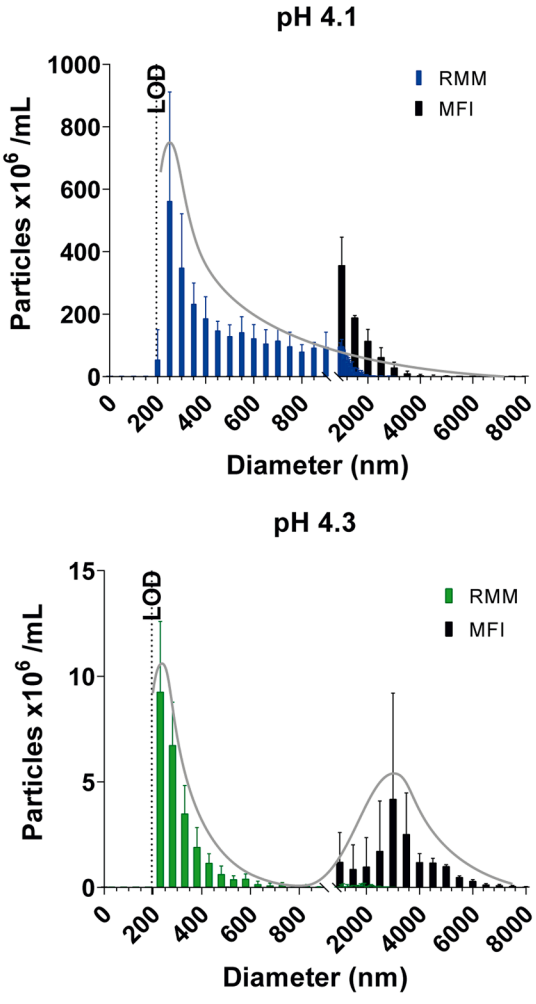

Fig. 3. Size and propensity of particulates formed at pH 4.1 (top) or 4.3 (bottom) combining the orthogonal methods Resonant Mass Measurements (RMM, coloured histograms) and Micro Flow Imaging (MFI, black histograms). The limit of detection (LOD) for the RMM is marked by a stippled line at 200 nm and the grey lines are added to illustrate the main distribution(s) for each pH. The error bars denote standard deviation of three independent measurements.

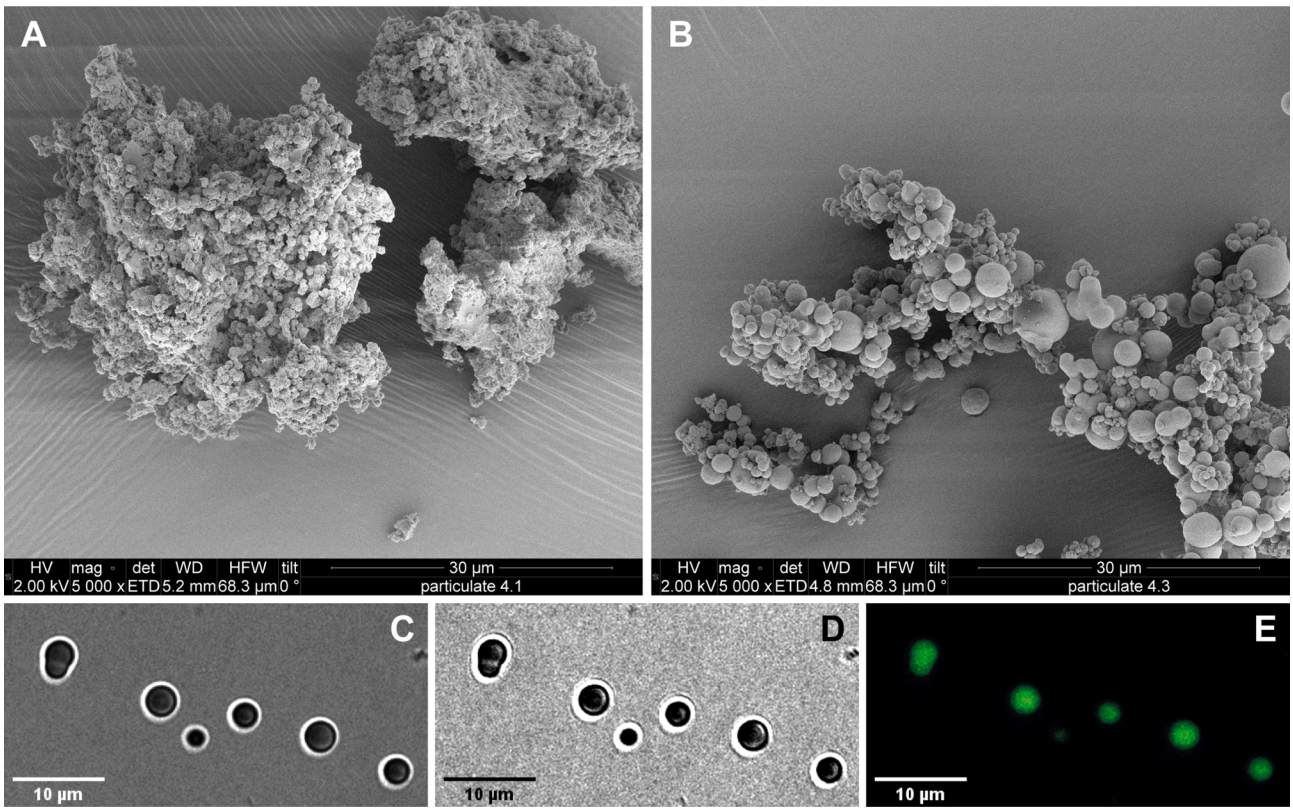

Fig. 4. Morphological analysis of the formed particulates after 24 h of heat stress. Scanning Electron Microscopy images of particulates formed at A) pH 4.1 or B) pH 4.3. Particulates formed at pH 4.3 were further investigated using C) optical microscopy, D) polarized light and E) fluorescence microscopy. For the fluorescence microscopy image, the particles were stained with the amyloid sensitive dye ThioflavinT.

only 12% of the total number of detected particles have a size below 2 µm, while 87% of the particulates resides in the size range 2–8 µm (Fig. S6). The shift can also be observed by qualitatively looking at representative MFI images of the detected particles in Fig. 2B, where individualized round-shaped particles are visible for both pH 4.1 and pH 4.3 samples, with the latter clearly showing particles with an increased size compared to pH 4.1. Moreover, the samples showed to be highly homogeneous with only 1–2% larger structures, which are not identified as particulates (Fig. S6 and S7).

The data in Fig. 1 and Fig. 2 indicate a dramatic effect due to only small changes in the pH. The occurrence of larger particles at pH 4.3 may be driven by fast coalescence phenomena due to the suppression of electrostatic interactions as observed for lysozyme close to the pI [13,46]. At pH 4.1, we can hypothesize that the charge on the protein may become more pronounced than at pH 4.3, so that the process is controlled by both the colloidal and conformational stability of the proteins. Further dedicated studies should be performed to test this hypothesis. Importantly, a similar effect was observed by Chaaban et al. [45] upon stressing human insulin in conditions containing different Hofmeister salts.

3.4. Nanosized particulates have more β-sheet content than micronsized particulates

The use of MFI gives an overview of particles with size > 1 µm. To probe subtle differences in the range of hundreds of nanometres and cover the full ranges of sizes, we performed Resonant Mass Measurements (RMM), which is suitable for size measurements in the range from 200 nm to 5 µm. Results are presented in Fig. 3 together with the MFI distribution for both pH 4.1 and pH 4.3.

The data shows that in both samples we have particles in the order of hundreds of nm, this component being much more significant at pH 4.1, where approximately 60 times as many particles are formed in the size range 200–300 nm, compared to pH 4.3. Adding the MFI measurement results (black histograms in Fig. 3) to the RMM data revealed that the pH 4.1 sample primarily consists of nanosized particulates with a tail reaching the low-micrometre range, whereas the pH 4.3 sample contains two distinct size populations. One population residing in the nanometre range, similar to the particulates formed at pH 4.1, and one population in the low-micrometre range centred around 3.5 µm. However, since the majority of the insulin mass is converted into the micron sized particulates, this particle fraction is truly dominating in the pH 4.3 sample. This highlights a pronounced relative size difference in the aggregate population under otherwise identical experimental conditions. Moreover, since the native-to-aggregation conversion rate is slightly higher at pH 4.3 compared to pH 4.1 (Fig. 1A), one could expect that at pH 4.1 we have more aggregates reaching a smaller size than the few ones formed at pH 4.3.

The difference in sizes for both samples is also clear from the morphological analysis performed by SEM (Fig. 4). Smaller particles in the range of 1–2 µm and below occur in the sample at pH 4.1 (Fig. 4A), while the presence of larger and more well-defined spherical particles with a diameter spanning from 1 to 10 µm is observed at pH 4.3 (Fig. 4B). We attribute the apparent particle–particle clustering to the increased stress time of 24 h for this analysis type. This ensured that adequate protein material was present during measurements. Moreover, the ultra-high vacuum during SEM measurements can cause clustering as well as particle rupture.

Representative individualized micronsized particles show a spherical shape under optical microscopy (Fig. 4C). Polarized light can provide information on the internal arrangement of the proteins in the formed particles. The technique has been utilized for other superstructures such as spherulites, whose internal symmetry gives rise to a “Maltese cross” [1,14]. We did not observe such pattern, indicating that the formed

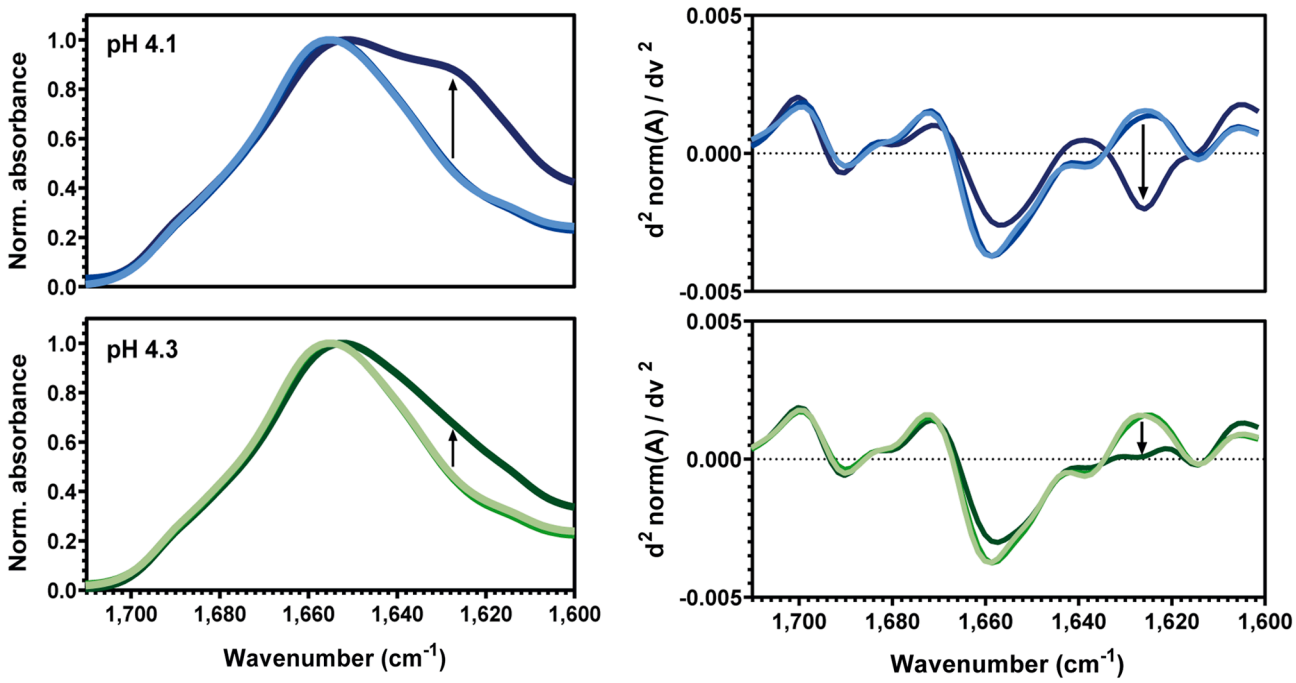

Fig. 5. Secondary structure characterization using FTIR spectroscopy of unstressed protein (bright colors), supernatant containing residual soluble insulin after stress application (medium colors) and pellet containing the formed particulates (darkest colors) for samples prepared at pH 4.1 (blue spectra) or pH 4.3 (green spectra). Both the normalized absorbance spectra (left) and the corresponding secondary derivative spectra (right) are shown, where arrows indicate an increase in aggregated β-sheet for the pellets around 1627 cm^{-1} compared to the unstressed protein sample. Each spectrum is an average of three independent preparations.

particulates do not exhibit any specific geometrical internal arrangement (Fig. 4D). Additionally, we found that they presented a fluorescence response when incubated with Thioflavin T (Fig. 4E), the latter suggesting the potential presence of β-sheet structure and an arrangement of amyloid-like origin.

Secondary structure analysis of the samples by FTIR spectroscopy highlights a difference between the particulates formed at the two pH values (Fig. 5). While both the unstressed protein sample and the residual soluble insulin after aggregation present a native-like spectrum with a main peak at 1656 cm^{-1}, the particulates show an increased infrared signal around 1627 cm^{-1}, which is ascribed to the formation of aggregated β-sheet (Fig. 5, arrows). The occurrence of this structural element is well aligned with the observed positive ThT signal for the particulates (Fig. 4E). Moreover, as also indicated by the second derivative of the FTIR spectra, the aggregate bands are more pronounced for the particulates formed at pH 4.1. This indicates that conformational change may occur more readily in such a condition, supporting the hypothesis that at pH 4.1 the unfolding process may be the rate-limiting step of the reaction.

4. Conclusions

In this study, we report that subtle changes around pH 4.0 for insulin has a dramatic effect on particulate kinetics, size and secondary structure. The negligible repulsive force closer to the pI mainly favours the formation of a micronsized population of particles. Moving further away from the pI activates a different pathway, with the formation of particles rich in β-sheet structures with a size mainly in the nanosize range.

Our results have a two-fold importance. On one hand, we highlight the importance of having a full control of the physicochemical parameters (such as pH) of the formulation. Moreover, applying a set of approaches analysing different length and time scales enables the isolation of different features of the aggregates. This allows obtaining single species aggregates which is a key aspect for the systematic and correct assessment of particle characteristics responsible for immunogenicity risk.

Declaration of Competing Interest

The authors declare that they have no known competing financial interests or personal relationships that could have appeared to influence the work reported in this paper.

Acknowledgements

CT, MBN, MG and VF acknowledge Novo Nordisk A/S for project funding and providing protein material. VF, AMS and CT acknowledge VILLUM FONDEN for supporting the project via the Villum Young Investigator Grant "Protein Superstructures as Smart Biomaterials (ProSmart)" 2018 – 2023 (Grant 19175).

The authors thank the VILLUM FONDEN (Grant 19175) for funding the CLARIOstar plate reader and VILLUM FONDEN (Grant 19175), the Novo Nordisk Foundation (Grant NNF16OC0021948), and Lundbeck Foundation (Grant R155-2013-14113) for funding the Leica DMi8 microscope. For use of SEM, authors acknowledge the Core Facility for Integrated Microscopy, Faculty of Health and Medical Sciences, University of Copenhagen and Jesper Søndergaard Marino from Novo Nordisk A/S for use of MFI image evaluation software.

Appendix A. Supplementary material

Supplementary data to this article can be found online at https://doi.org/10.1016/j.ejpb.2022.09.001.

References

[1] V. Vetri, V. Foderà, The route to protein aggregate superstructures: Particulates and amyloid-like spherulites, FEBS Lett 589 (2015) 2448–2463.
[2] C.G. Frankaer, P. Sonderby, M.B. Bang, R.V. Mateiu, M. Groenning, J. Bukrinski, P. Harris, Insulin fibrillation: The influence and coordination of Zn(2), J Struct Biol 199 (2017) 27–38.
[3] M.I. Smith, V. Foderà, J.S. Sharp, C.J. Roberts, A.M. Donald, Factors affecting the formation of insulin amyloid spherulites, J. colsurfb 89 (2012) 216–222.

[4] G. De Luca, D. Fennema Galparsoro, G. Sancataldo, M. Leone, V. Foderà, V. Vetri, Probing ensemble polymorphism and single aggregate structural heterogeneity in insulin amyloid self-assembly, J Coll Int Sci 574 (2020) 229–240.
[5] X. Zhou, D. Fennema Galparsoro, A. Ostergaard Madsen, V. Vetri, M. van de Weert, H. Morck Nielsen, V. Foderà, Polysorbate 80 controls Morphology, structure and stability of human insulin Amyloid-Like spherulites, J Coll Int Sci 606 (2022) 1928–1939.
[6] J. Brange, L. Andersen, E.D. Laursen, G. Meyn, E. Rasmussen, Toward understanding insulin fibrillation, J Pharm Sci 86 (1997) 517–525.
[7] M. Sunde, L.C. Serpell, M. Bartlam, P.E. Fraser, M.B. Pepys, C.C. Blake, Common core structure of amyloid fibrils by synchrotron X-ray diffraction, J Mol Biol 273 (1997) 729–739.
[8] M.R. Krebs, C.E. Macphee, A.F. Miller, I.E. Dunlop, C.M. Dobson, A.M. Donald, The formation of spherulites by amyloid fibrils of bovine insulin, PNAS 101 (2004) 14420–14424.
[9] M.R. Krebs, E.H. Bromley, S.S. Rogers, A.M. Donald, The mechanism of amyloid spherulite formation by bovine insulin, Biophys J 88 (2005) 2013–2021.
[10] D. Fennema Galparsoro, X. Zhou, A. Jaaloul, F. Piccirilli, V. Vetri, V. Foderà, Conformational Transitions upon Maturation Rule Surface and pH-Responsiveness of alpha-Lactalbumin Microparticulates, ACS Appl Bio Mater 4 (2021) 1876–1887.
[11] M.R. Krebs, K.R. Domike, A.M. Donald, Protein aggregation: more than just fibrils, Biochem Soc Trans 37 (2009) 682–686.
[12] J.E. Coleman, B.J. Allan, B.L. Vallee, Protein spherulites, Sci 131 (1960) 350–352.
[13] V. Foderà, V. Vetri, T.S. Wind, W. Noppe, C. Cornett, A.M. Donald, L.A. Morozova-Roche, B. Vestergaard, Observation of the Early Structural Changes Leading to the Formation of Protein Superstructures, J Phys Chem Lett 5 (2014) 3254–3258.
[14] K.R. Domike, E. Hardin, D.N. Armstead, A.M. Donald, Investigating the inner structure of irregular beta-lactoglobulin spherulites, Eur Phys J E 29 (2009) 173–182.
[15] M.C. Heijna, M.J. Theelen, W.J. van Enckevort, E. Vlieg, Spherulitic growth of hen egg-white lysozyme crystals, J Phys Chem B 111 (2007) 1567–1573.
[16] M.R. Krebs, G.L. Devlin, A.M. Donald, Protein particulates: another generic form of protein aggregation? Biophys J 92 (2007) 1336–1342.
[17] V. Foderà, A. Zaccone, M. Lattuada, A.M. Donald, Electrostatics controls the formation of amyloid superstructures in protein aggregation, Phys Rev Lett 111 (2013) 105–108.
[18] A. Ahmad, V.N. Uversky, D. Hong, A.L. Fink, Early events in the fibrillation of monomeric insulin, J Biol Chem 280 (2005) 42669–42675.
[19] V. Foderà, A.M. Donald, Tracking the heterogeneous distribution of amyloid spherulites and their population balance with free fibrils, Eur Phys J E 33 (2010) 273–282.
[20] A.S. Rosenberg, Effects of protein aggregates: an immunologic perspective, AAPS J 8 (2006) 501–507.
[21] J.S. Bee, T.J. Goletz, J.A. Ragheb, The future of protein particle characterization and understanding its potential to diminish the immunogenicity of biopharmaceuticals: a shared perspective, J Pharm Sci 101 (2012) 3580–3585.
[22] A.S. Rosenberg, A.S. Worobec, A Risk-Based Approach to Immunogenicity Concerns of Therapeutic Protein Products: Part 2, Considering Host-Specific and Product-Specific Factors Impacting Immunogenicity, BioPharm int. 17 (2004) 34–42.
[23] J. Kotarek, C. Stuart, S.H. De Paoli, J. Simak, T.L. Lin, Y. Gao, M. Ovanesov, Y. Liang, D. Scott, J. Brown, Y. Bai, D.D. Metcalfe, E. Marszal, J.A. Ragheb, Subvisible Particle Content, Formulation, and Dose of an Erythropoietin Peptide Mimetic Product Are Associated With Severe Adverse Postmarketing Events, J Pharm Sci 105 (2016) 1023–1027.
[24] A. Braun, L. Kwee, M.A. Labow, J. Alsenz, Protein aggregates seem to play a key role among the parameters influencing the antigenicity of interferon alpha (IFN-alpha) in normal and transgenic mice, Pharm Res 14 (1997) 1472–1478.
[25] A. Seidl, O. Hainzl, M. Richter, R. Fischer, S. Bohm, B. Deutel, M. Hartinger, J. Windisch, N. Casadevall, G.M. London, I. Macdougall, Tungsten-induced denaturation and aggregation of epoetin alfa during primary packaging as a cause of immunogenicity, Pharm Res 29 (2012) 1454–1467.
[26] J.G. Barnard, K. Babcock, J.F. Carpenter, Characterization and quantitation of aggregates and particles in interferon-beta products: potential links between product quality attributes and immunogenicity, J Pharm Sci 102 (2013) 915–928.
[27] H. Schellekens, Factors influencing the immunogenicity of therapeutic proteins, Nephrol Dial Transplant 20 (2005) 3–9.
[28] K.D. Ratanji, J.P. Derrick, R.J. Dearman, I. Kimber, Immunogenicity of therapeutic proteins: influence of aggregation, J Immunotoxicol 11 (2014) 99–109.
[29] S. Hermeling, L. Aranha, J.M. Damen, M. Slijper, H. Schellekens, D.J. Crommelin, W. Jiskoot, Structural characterization and immunogenicity in wild-type and immune tolerant mice of degraded recombinant human interferon alpha2b, Pharm Res 22 (2005) 1997–2006.
[30] W. Jiskoot, G. Kijanka, T.W. Randolph, J.F. Carpenter, A.V. Koulov, H.C. Mahler, M.K. Joubert, V. Jawa, L.O. Narhi, Mouse Models for Assessing Protein Immunogenicity: Lessons and Challenges, J Pharm Sci 105 (2016) 1567–1575.
[31] N. Benne, J. van Duijn, J. Kuiper, W. Jiskoot, B. Slutter, Orchestrating immune responses: How size, shape and rigidity affect the immunogenicity of particulate vaccines, J Control Release 234 (2016) 124–134.
[32] V. Filipe, W. Jiskoot, A.H. Basmeleh, A. Halim, H. Schellekens, V. Brinks, Immunogenicity of different stressed IgG monoclonal antibody formulations in immune tolerant transgenic mice, MAbs 4 (2012) 740–752.
[33] E.M. Moussa, J.P. Panchal, B.S. Moorthy, J.S. Blum, M.K. Joubert, L.O. Narhi, E. M. Topp, Immunogenicity of Therapeutic Protein Aggregates, J Pharm Sci 105 (2016) 417–430.
[34] A.J. Freitag, M. Shomali, S. Michalakis, M. Biel, M. Siedler, Z. Kaymakcalan, J. F. Carpenter, T.W. Randolph, G. Winter, J. Engert, Investigation of the immunogenicity of different types of aggregates of a murine monoclonal antibody in mice, Pharm Res 32 (2015) 430–444.
[35] B. Boll, J. Bessa, E. Folzer, A. Rios Quiroz, R. Schmidt, P. Bulau, C. Finkler, H. C. Mahler, J. Huwyler, A. Iglesias, A.V. Koulov, Extensive chemical modifications in the primary protein structure of IgG1 subvisible particles are necessary for breaking immune tolerance, Mol Pharm 14 (2017) 1292–1299.
[36] G. Kijanka, J.S. Bee, S.A. Korman, Y. Wu, L.K. Roskos, M.A. Schenerman, B. Slutter, W. Jiskoot, Submicron size particles of a murine monoclonal antibody are more immunogenic than soluble oligomers or micron size particles upon subcutaneous administration in mice, J Pharm Sci 107 (2018) 2847–2859.
[37] M.K. Joubert, M. Hokom, C. Eakin, L. Zhou, M. Deshpande, M.P. Baker, T.J. Goletz, B.A. Kerwin, N. Chirmule, L.O. Narhi, V. Jawa, Highly aggregated antibody therapeutics can enhance the in vitro innate and late-stage T-cell immune responses, J Biol Chem 287 (2012) 25266–25279.
[38] C. Thorlaksen, M.S. Neergaard, M. Groenning, V. Foderà, Reproducible formation of Insulin Superstructures: amyloid-like fibrils, spherulites and particulates, protein aggregation: methods and protocols, Methods mol. biol, SpringerNature, 2022.
[39] J.S. Pedersen, M. Persson, Unmasking translucent protein particles by improved micro-flow imaging algorithms, J Pharm Sci 103 (2014) 107–114.
[40] A.D. Grabarek, D. Weinbuch, W. Jiskoot, A. Hawe, Critical evaluation of microfluidic resistive pulse sensing for quantification and sizing of nanometer- and micrometer-sized particles in biopharmaceutical products, J Pharm Sci 108 (2019) 563–573.
[41] A.B. Krueger, J. Hadley, P.P. Cheney, N. Markova, J.F. Carpenter, A.H. Fradkin, Application of a best practice approach using resonant mass measurement for biotherapeutic product characterization, J Pharm Sci 108 (2019) 1675–1685.
[42] E. Folzer, T.A. Khan, R. Schmidt, C. Finkler, J. Huwyler, H.C. Mahler, A.V. Koulov, Determination of the density of protein particles using a suspended microchannel resonator, J Pharm Sci 104 (2015) 4034–4040.
[43] J. Brange, D.R. Owens, S. Kang, A. Volund, Monomeric insulins and their experimental and clinical implications, Diabetes Care 13 (1990) 923–954.
[44] M.M. Schack, E.H. Moller, J.F. Carpenter, T. Rades, M. Groenning, A Platform for preparing homogeneous proteinaceous subvisible particles with distinct morphologies, J Pharm Sci 107 (2018) 1842–1851.
[45] H. Chaaban, J.J. Vallooran, M. van de Weert, V. Foderà, Ion-Mediated morphological diversity in protein amyloid systems, J Phys Chem Lett (2022) 3586–3593.
[46] K. Pounot, H. Chaaban, V. Foderà, G. Schirò, M. Weik, T. Seydel, Tracking internal and global diffusive dynamics during protein aggregation by high-resolution neutron spectroscopy, J Phys Chem Lett 11 (2020) 6299–6304.